Modelling the resonant frequency associated with the spatio-temporal evolution of the bone-dental implant interface

Sapir Gershov [1], Jing XIE [2], Furqan A. Shah [3], Keren Shemtov-Yona [4,5], Daniel Rittel [4]

1. Technion Autonomous Systems Program, Technion - Israel Institute of Technology, 32000 Haifa, Israel
2. State Key Laboratory of Explosion Science and Technology, Beijing Institute of Technology, 100081 Beijing, China
3. Department of Biomaterials, Sahlgrenska Academy, University of Gothenburg, Göteborg, Sweden
4. Faculty of Mechanical Engineering, Technion - Israel Institute of Technology, 32000 Haifa, Israel
5. The Maurice and Gabriela Goldschleger School of Dental Medicine, Department of Oral Biology, Tel Aviv University, 39040 Tel Aviv, Israel

Corresponding author:

Sapir Gershov, sapirgershov@campus.technion.ac.il, +972-502360623

Technion Autonomous Systems Program, Technion - Israel Institute of Technology, 32000 Haifa, Israel

Abstract

Dental implant stability is greatly affected by the mechanical properties of the bone-implant interface (BII), and it is key to long-term successful osseointegration. Implant stability is often evaluated using the Resonant Frequency Analysis (RFA) method, and also by the quality of this interface, namely the bone-implant contact (BIC). True to this today, there is a scarcity of models tying BIC, RFA and a spatially and mechanically evolving BII.

In this paper, based on the contact/distance osteogenesis concept, a novel numerical spatio-temporal model of the implant, surrounding bone and evolving interface, was developed to assess the evolution of the interfacial stresses on the one hand and the corresponding resonant frequencies on the other.

We postulate that, since the BIC percentage reaches saturation over a very short time, long before densification of the interface it becomes irrelevant as to load transmission between the implant and the bone, due to the existence of an open gap. Gap closure is the factor that provides continuity between the implant and the surrounding bone.

The results of the calculated RFA evolution match and provide an explanation for the multiple clinical observations of a sharp initial decline in RFA, followed by a gradual increase and plateau formation.

Keywords: Bone Implant Interface, Osteointegration, Bone Implant Contact, Numerical Simulation, Radio Frequency Analysis

1. Introduction

Dental implant stability is affected by the mechanical properties of the connection between the implant and the bone, also known as the bone-implant interface (BII). Although the optimal biomechanical properties of the BII have not yet been fully clarified, it is known that the BII determines the mobility of the implant, whose limitation is a requisite for successful osseointegration. Osseointegration is defined as a direct connection between living bone and implants that can provide structural support[1,2] and without it, long-term success cannot be achieved. Implant stability is viewed as a two-step process: (1) Primary, which mostly results from mechanical attachment with the cortical bone, and (2) Secondary, which involves bone regeneration and remodeling, and is affected by primary stability[3].

A study by Søballe et al[4], has shown that implant micromotions during healing may affect the process of osseointegration and bone remodeling. Micromotion of 50 – 150 μm may cause fibrous tissues formation at the BII, inducing bone resorption. This shows that primary stabilization of the implant in bone tissue is a necessary condition for successful implant osseointegration. In other words, the absence of mobility in the bone bed after implant placement, is of utmost importance for the long-term success of dental implants.

Despite their widespread clinical use, failures of dental implant integration still occur and remain difficult to anticipate. There is a great need for continuous monitoring of the implant stability status, specifically during the healing phase, quantitatively and objectively. A proper evaluation during the early stages of recovery can provide insight and essential information that will substantially help in improving the long-term prognosis of dental implants[3].

Numerous methods have been employed overall the last decades to identify implant stability. These methods can be categorized as invasive and non-invasive. Historically, the gold standard method to evaluate stability is bone histomorphometry. Bone histomorphometry is the assessment of cellular and structural variables through histological section observation, and it is an essential technique for monitoring changes at the tissue-level of mechanisms pertaining to bone physiology[5,6]. These measures are obtained by calculating the 2D bone-implant contact (BIC) percentage on histological sections. Higher BIC values, i.e., a larger amount of bone in contact with the implant, results in a higher structural stiffness. The BIC is correlated with the biomechanical properties of the BII and increases during bone healing[7].

However, due to the invasive and destructive procedure, bone histomorphometry is not suitable for in-vivo long-term studies or clinical continuous monitoring[8]. Moreover, during the healing process, the generated woven bone is poorly organized. Its composition and mechanical properties

constantly evolve[9,10], and therefore it is a challenging task to quantify them at the onset of the healing phase.

Based on the available literature, there is virtually no documentation regarding human dental BIC measurements at the early stages of the healing period. To the best of our knowledge, the earliest documented period for dental implant in humans was 4 weeks after the surgery[11,12]. This scarcity of published results is consistent with the difficulty to evaluate woven bone properties using bone histomorphometry.

Resonance Frequency Analysis (RFA)[13] is an alternative method to measure the initial stability of an implant in a non-destructive manner, and has gradually become a common clinical method[14–16]. RFA consists of measuring the resonant frequency(ies) of a dental implant that is actuated externally by means of electromagnetically induced vibrations. The results are converted into an Implant Stability Quotient (ISQ)[17], whose exact definition is not very clear. Yet, the higher the ISQ value based on the resonant frequency, the higher the stability[18]. The resonance frequency analysis depends upon three main aspects: (1) the design of the transducer itself; (2) the total effective length of the implant above the marginal bone level (super crestal); (3) the stiffness of the implant fixture and its BII[17,19]. Several papers have questioned the existence of a significant correlation between RFA measurements and BIC in human specimens[8,20–23]. Therefore, the relation between implant stability, as obtained from RFA measurements, and BIC is still an open/controversial subject.

The use of finite element analysis (FEA) in biomechanics, and especially in dental biomechanics, is increasingly becoming a popular alternative/complement for “hands-on” measurement. Performing FE analyses of the BII requires a proper description of its mechanical behavior, assuming different hypotheses about the biological tissue and the interlocking of implant surface[24]. Until recently, the very nature of the BII was simplified, either by assuming a perfectly bonded or an equivalent frictional state, overlooking the fact that a dental implant is never fully bonded[25,26], akin to 100% BIC. In addition, these models don’t include the complex nature of the bone or the temporal evolution of stiffness of the BII zone[26].

In a recent paper by Xie et al.[26], a simple, yet physically-informed model, was presented for the mesoscale mechanical characteristics of the BII. The numerical study provided spatial-temporal evolution of discrete elements and the overall model mechanical response. By tracking each cubic micrometer of bone throughout the process of peri-implant osteogenesis, the authors extracted the biomechanical properties of the BII region over time. However, this model did not consider the BIC itself as it concerned only the interfacial layer (BII). In this work, the concepts of contact and distance osteogenesis (CO and DO, respectively), were implemented to describe the evolution of the moving bone densification fronts from and towards the implant[27].

Xie et al.'s model[26] clearly shows that as long as the CO and DO fronts have not met (i.e., before gap closure), the interface (BII) offers no significant elastic resistance to loadings. In other words, the BII cannot transfer stress between the remote (DO) bone part and the implant as it offers no mechanical resistance. Load transfer can only occur significantly once the gap between CO and DO is closed, which may take some 30 days or more, according to the assumed CO/DO kinematics. The above reasoning raises an interrogation about the mechanical characterization of the BII in the early period that precedes gap closure and complete "solidification" of the BII.

With such a model for the BII at hand, and despite its simplifications, one can now introduce the BII and its evolution explicitly into a finite element model of the bone-implant system, to determine the overall mechanical response of the bone-implant system and its corresponding resonant frequency. For such a task, one needs to carefully examine the components influencing the BII mechanical behavior: (1) BII stiffness, and (2) BIC expressing the degree of attachment of the bone to the dental implant.

Consequently, the goal of this research is to numerically assess the influence of a spatially and mechanically evolving BII, in parallel with the evolution of the BIC, on the implant-bone load transmission, thereby defining the limits of detectability of mechanical changes, that could be assessed using the Resonance Frequency Analysis or any other method.

2. Modelling considerations

2.1. BII stiffness considerations

The study of Xie et al.[26] describes Young's modulus evolution in time under different assumed evolutions of contact and distance osteogenesis[27] (CO and DO, respectively), represented schematically in Figure 1.

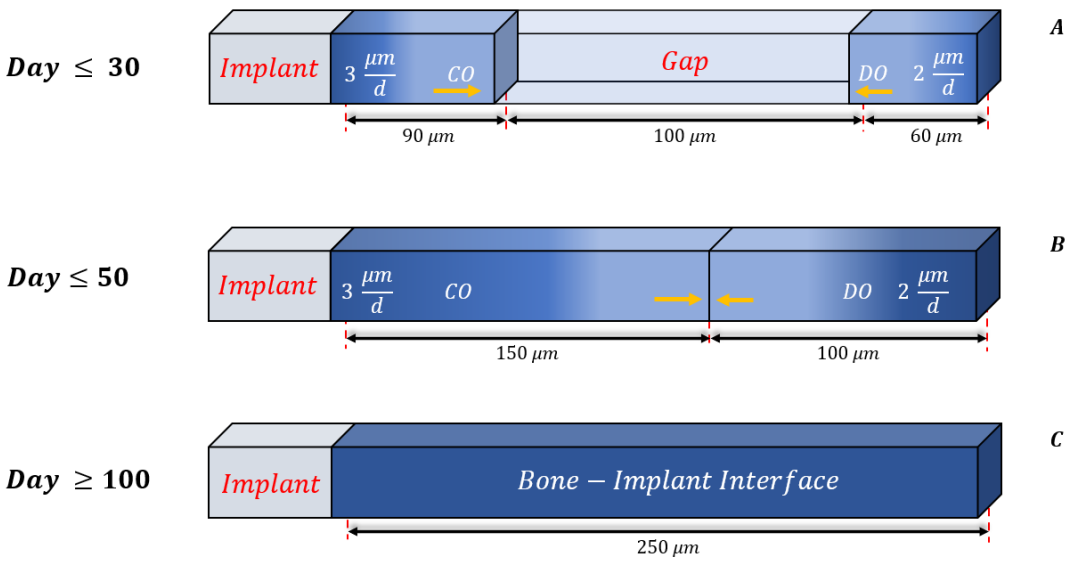

Figure 1: Schematic representation of the BII kinetics use white color for Bone-implant interface

The schematic representation of the BII (Figure 1) features 3 distinct domains:

(1) The connection between the implant and the bone, is embodied in the evolving BIC and CO.

(2) The evolving remote osseointegration front, is embodied in the DO region.

(3) The bone material between the CO and the DO regions progresses towards each other with time until ultimate gap closure (Figure 1, B) and generation of a solid bone (Figure 1, C).

2.2. BIC considerations

Based on the accumulated knowledge and experience, it appears that the BIC is a critical factor for long-term implant success[28]. As mentioned, the BIC is quantified by measuring the amount of the implant surface directly attached to the mineralized bone. Traditionally, the measurement is done without the interposition of soft connective tissue[28].

There is a vast amount of literature documenting the BIC values of the dental implant, and specifically for humans. However, due to the difficulty in performing histomorphometry analysis during the early stages of bone healing, there is no literature that can provide BIC measurements during the first days / weeks of the healing phase. The following focuses on papers that have reported measurements from the early stages of the healing, i.e. 4 – 28 weeks after surgery[11,12,37–46,29,47–49,30–36]. For every paper, the reported measurement is the average value. When several sources reporting BIC of the same time interval were found, the average BIC was calculated (Table 1).

Weeks	Average BIC (%)	Ref.
4	58.76	11, 12
5	53.15	11, 29
6	82.33	11
7	55.00	43
8	46.63	11, 12, 31-40, 48
16	79.77	41, 42
24	63.17	43-47
28	55.00	49

Table 1: Partial summary of the average human BIC reported in the literature.

Due to the lack of information regarding the first week of the healing period, the first data point of

the curve is arbitrarily set to (0, 10) (i.e., the BIC of the first week is set to 10%).

Based on the accumulated measurements and the added starting point, we constructed a mathematical equation that estimates the BIC as a function of time ($BIC\% = f(t)$).

The function is written as follows:

$$BIC\% = a \cdot \mathrm{erf}(b \cdot t + c) + d \quad (1)$$

With coefficients (with 95% confidence bounds) listed in Table 2:

a	b	c	d	R^2
24.8	0.9157	−3.134	36.8	0.7016

Table 2: The values of Equation (1) coefficients

The following graph are constructed using Equation (1) for different time intervals:

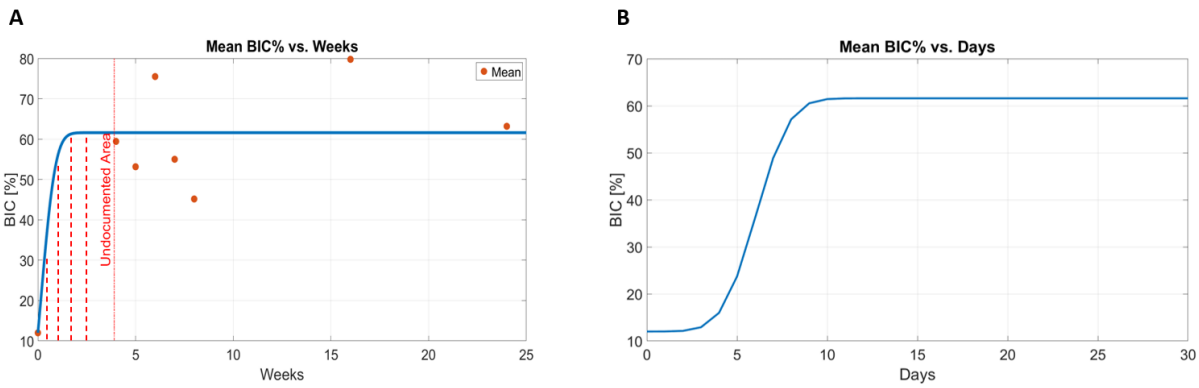

Figure 2: The BIC evolution. (A) values from the literature and (B) the model (Eqn. (1))

Figure 2-A illustrates the average BIC as reported in the available literature and the BIC curve constructed from these data points. The curve fit is reported in table 2. Notice that the first 4 weeks are undocumented, and the BIC evolution is therefore assumed for the sake of continuity.

Figure 2-B illustrates the numerically estimated average BIC during the first 4 weeks, i.e., the undocumented area. The curve is calculated using Equation (1). The BIC curve has a sigmoid-like shape where the first data point is arbitrarily set to (0, 10) and continuously rises until it reaches a plateau after approximately 12 days.

2.3 Coupling the BII stiffness and BIC

Noting that the BIC percentage and BII stiffness evolve in parallel, one can now couple the two as shown in Figure 3.

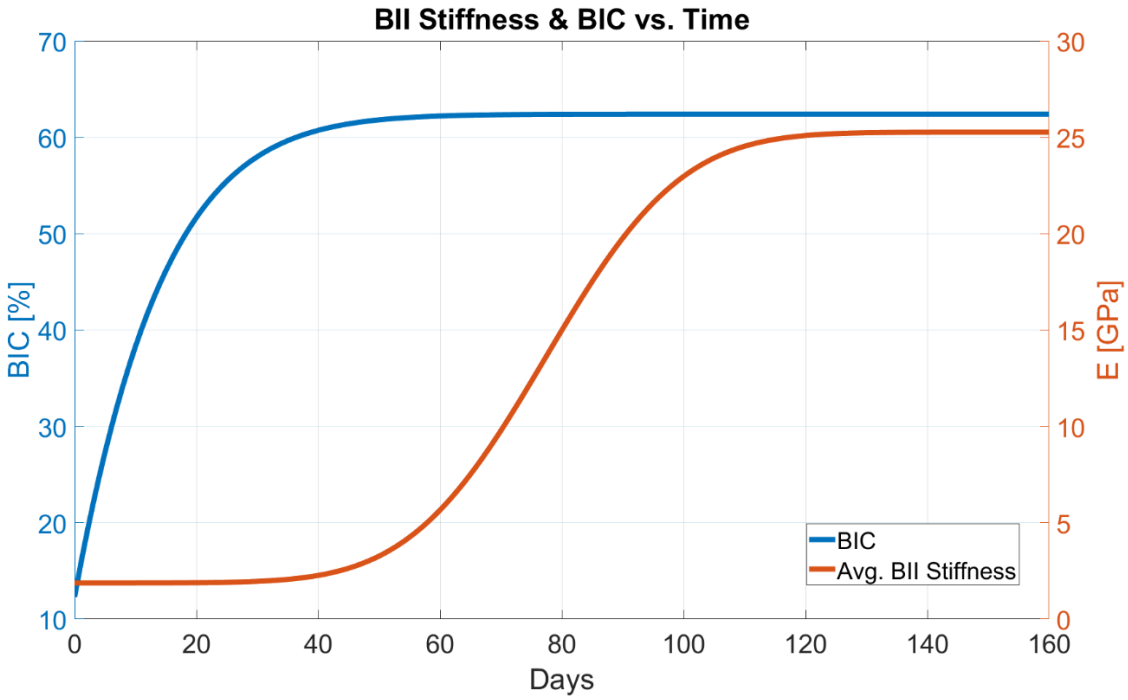

Figure 3: BII stiffness and BIC as a function of time. The average BII stiffness represents the evolution of resultant stiffness at constant DO but varies according to Xie et al.[26]

Since both the BIC and the interfacial stiffness evolve with time, one can express the stiffness of an interfacial element unit as a function of its BIC ratio, thereby yielding a more realistic mechanical representation of the BII. Based on the work of Xie et al.[26], a mathematical model that couples the stiffness of an interfacial element unit with respect to the BIC was devised (Figure 3).

When taking into consideration the curves in Figure 3 and the results from Xie et al.[26] (Figure 1) one can easily deduce the following:

(1) During the first stages of the osteointegration process, days 0 – 30, the BIC is rapidly growing while the BII stiffness is essentially constant around 1.87 GPa. This time interval correlates with Figure 1-A, where there is a gap between the CO and DO fronts. This implies that during that period, the BIC is the primary measurement to assess the implant stability, while the process of estimating the BII stiffness is of little relevance since there is an open gap between the implant and the bone for which the *averaged* stiffness is continuously the lowest until gap closure.

(2) In Figure 3, during days 50 – 100, there is a shift in the curves, and from that point on, the BII stiffness is increasing until it reaches a plateau while the BIC remains constant. This time interval correlates with Figure 1-B, where the gap between the CO and DO fronts is closed.
This implies that during that period, the BII stiffness is the primary measurement to assess the implant stability, while the BIC becomes constant.

3 Materials and methods

The model is composed of an MIS Seven (Seven® MIS, Barlev, Israel) implant[50], the (evolving) interface, and the solid bone (Figure 4). For the implant, isotropic mechanical properties of Ti-6Al4V ELI (American Society for Testing and & American Society for Testing and Materials 2013) were used (see Table 2). Cortical and trabecular bone tissues were assumed to be isotropic with mechanical properties according to Guan et al.'s work[51] (Table 2).

Material	Young's Modulus $E\ [GPa]$	Poisson's ratio υ	Density $\rho\ \left[\frac{kg}{m^3}\right]$
Ti-6Al4V ELI	113.8	0.33	4430
Cortical bone	18	0.35	1900
Trabecular bone	0.7	0.34	1000

Table 2: Mechanical properties of the FE model static components

The model is three dimensional, where each unit cell is assumed to behave as a linear elastic isotropic material while the simulation of the spatially and mechanically evolving BII is dynamic (i.e., changes during the simulation based on the model in Figure 3). The analysis was carried out using the commercial finite element package Abaqus/Explicit (version 6.14, Simulia, Providence, RI)[52].

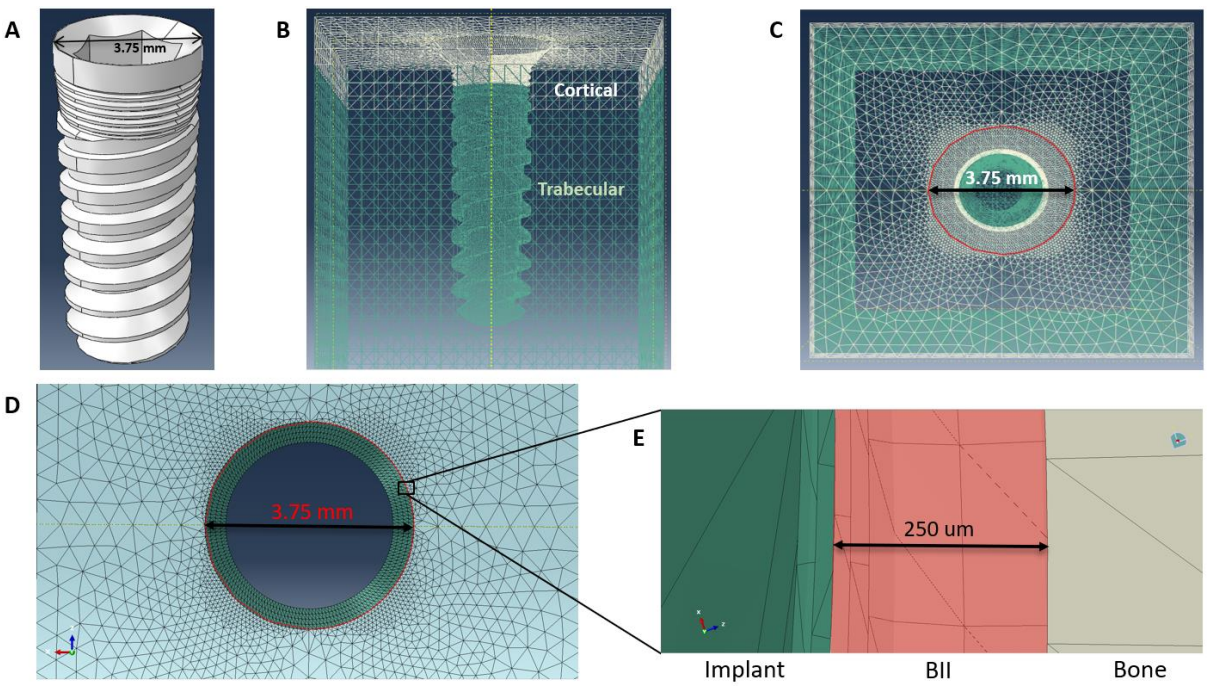

Figure 4: FE model. A – MIS Seven implant; B – The meshed bone & implant model; C – Top view of the model's mesh with a 250 μm wide BII (marked in red); D – Magnification of the BII region (red); E - Details of the interfacial mesh

To properly model a spatially and mechanically evolving interface, an initial FE model was constructed to represent the process described in Figure 1-A. More specifically, we assigned the CO and DO fronts, and BII layers from the implant and bone respectively, with the kinematics of $3\,\frac{\mu m}{day}$ and $2\,\frac{\mu m}{day}$ respectively. Due to software limitations, the *initial* width of the CO layer is 6-micron, and the DO layer is 4-micron. The initial gap between the two fronts is therefore 240-micron wide. The process of CO and DO evolution is embodied by the change in the element's mechanical properties at each time step. The external boundary of the cortical and trabecular components is constrained in all directions.

Once the initial spatial properties are set, a dedicated routine composed of the following four steps is applied:

(1) First, the coupled model of stiffness and BIC as a function of time is assigned to the 6-micron wide interfacial CO layer (Figure 4 A-B). A CO of width 6-micron and DO of 4-micron are equivalent to 2 days of osteointegration, according to the prescribed speeds of progression of each front. As for the gap between the two fronts, we assign the lowest stiffness value of 1.87 GPa, which could as well be 0 since the interface offers no significant mechanical resistance, as it is not comprised of solid matter.

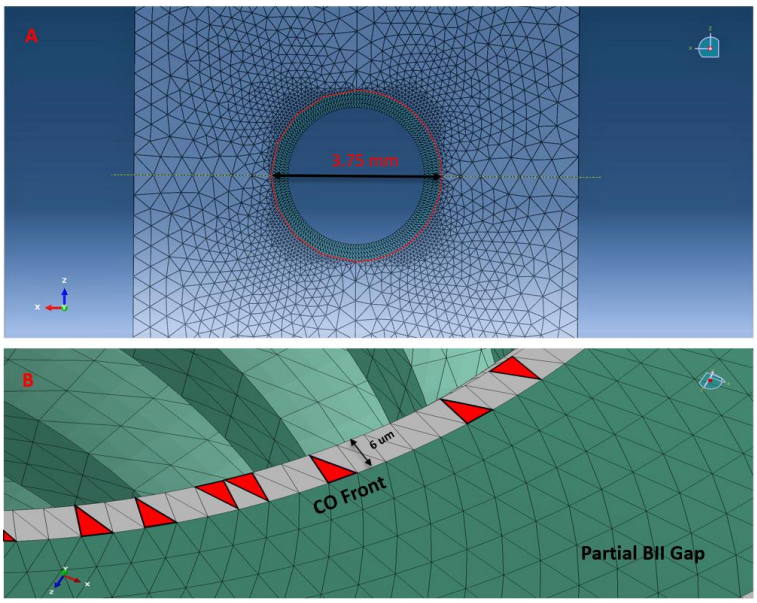

Figure 5: Illustration of the BII CO front of 6-micron width. BII-CO front of 6-micron (2nd day for illustration). All elements that are common to the implant and the BII CO front are colored in grey. implant osteotomy and BII gap, are colored in green. A randomly selected number of elements of the BII on the CO side are colored in red

(2) To compose the BIC, elements that are common to the implant and the BII CO side are selected

randomly (Figure 5B). The BIC is represented by the number of such randomly selected BII CO elements divided by the total number of common elements. As for the DO side, there is no random selection, and all elements participate in the simulated evolution. The BIC and the interfacial stiffness as a function of the time are iteratively updated according to Figure 4. A total of 10 realizations per BIC percentage were modelled.

(3) At each iteration, a 100 N force, making a 35-degree angle with the longitudinal implant axis is applied and peri-implant stresses are thus calculated.

(4) For the same configuration, the resonance frequency of the bone-implant ensemble is calculated next (for the most relevant first mode).

4. Data analysis

During the implantation process, an osteotomy is first practiced by drilling into the jawbone with a diameter that is inferior to that of the implant. Next, the implant is screwed into the osteotomy, creating a replica of the implant thread into the bone. After a short period of time, during which the damaged bone dissolves and stresses relax, thus creating the initial assumed 250-micron wide gap, the bone starts reconstructing itself with the above-mentioned CO/DO processes. A shown in Figure 6, it is assumed that the initial geometry of the bone thread perfectly matches that of the implant and that the time for the onset of the BII formation is at which the CO/DO processes start.

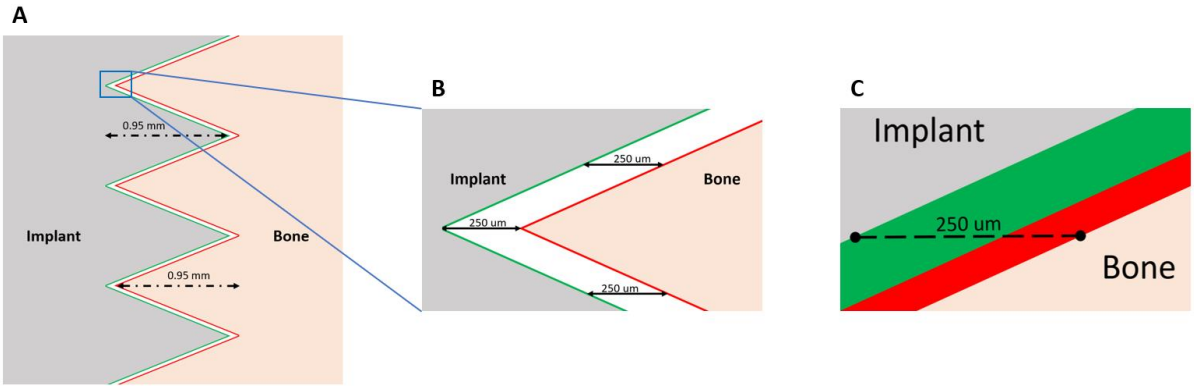

Figure 6: Illustration (out of scale) of the symmetry assumption.

The outer line of the implant, colored in green, is the CO layer of the BII. The outer line of the bone, colored in red, is the DO layer of the BII. Figure A depicts the evolution of the BII layer on day 0 (each front has a width of 0 um) and Figure B is a more detailed illustration. Figure C depicts the BII on day 50 - no gap between the CO and DO (i.e., complete contact between all elements of the CO and the DO distal fronts)

Our calculations start on day 2, due to software limitations, where the gap size is reduced to 240-micron.

The following procedure was applied to calculate the interfacial stresses of the evolving model:

(1) Elements were divided onto 3 distinct categories: (a) CO elements - all elements that lie between the implant surface and the CO front; (b) DO elements - all elements that lie between the bone surface and the DO (c) Gap elements – all elements that lie between the CO and DO fronts. As mentioned earlier in the simulation dedicated routine, the elements of each category are assigned with the appropriate mechanical properties.

(2) To properly calculate the von Mises stress in the BII as a function of time during the first 50 days, one must calculate the average stress for each section (CO, DO and gap).

(3) For the CO and DO elements we define a sub-category as follows: all main category elements (CO elements and DO elements) that are located in the distal front of the layer are considered as "shell elements" (Figure 7).

(4) Next, the averaged von Mises stress on those "shells" can be plotted as a function of the distance, thus reflecting the assumed evolution of the CO-DO fronts.

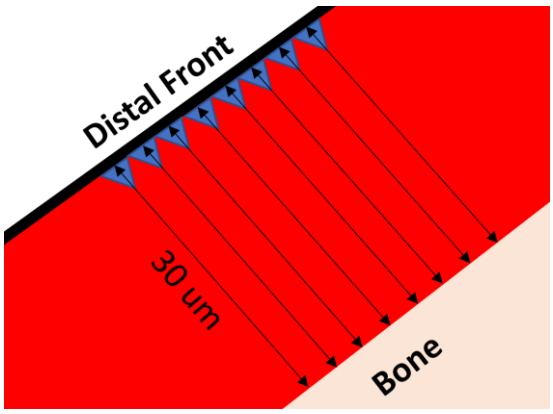

Figure 7: Partial illustration (out of scale) of the "shell elements" (blue triangles).

(5) As for the gap, we calculate the average stress based on all elements confounded in this region. I.e., we calculate the gap elements' average stress.

(6) We repeat stages 3 – 5 until the gap is closed (all distal elements are in contact).

(7) After 50 days, once the gap is closed, the calculation of the average Mises stress can be performed on the complete model (i.e., the sum of all stresses divided by the total number of elements).

(8) Finally, the resonant frequency (first mode) is calculated for the model using the standard procedure detailed in[15].

5. Results

In the following section we will present the results for the von Mises stress and the RFA, generated from the described simulation and data analysis. The results were calculated in a Python 3.8 environment.

5.1 von Mises stresses as a function of time and distance

The von Mises stress results were calculated individually in every time step, based on the process described in materials and methods and the data analysis sections. The von Mises stress is the simplest scalar representation of the acting stresses. The following Figure is the combination of these results in a single graph.

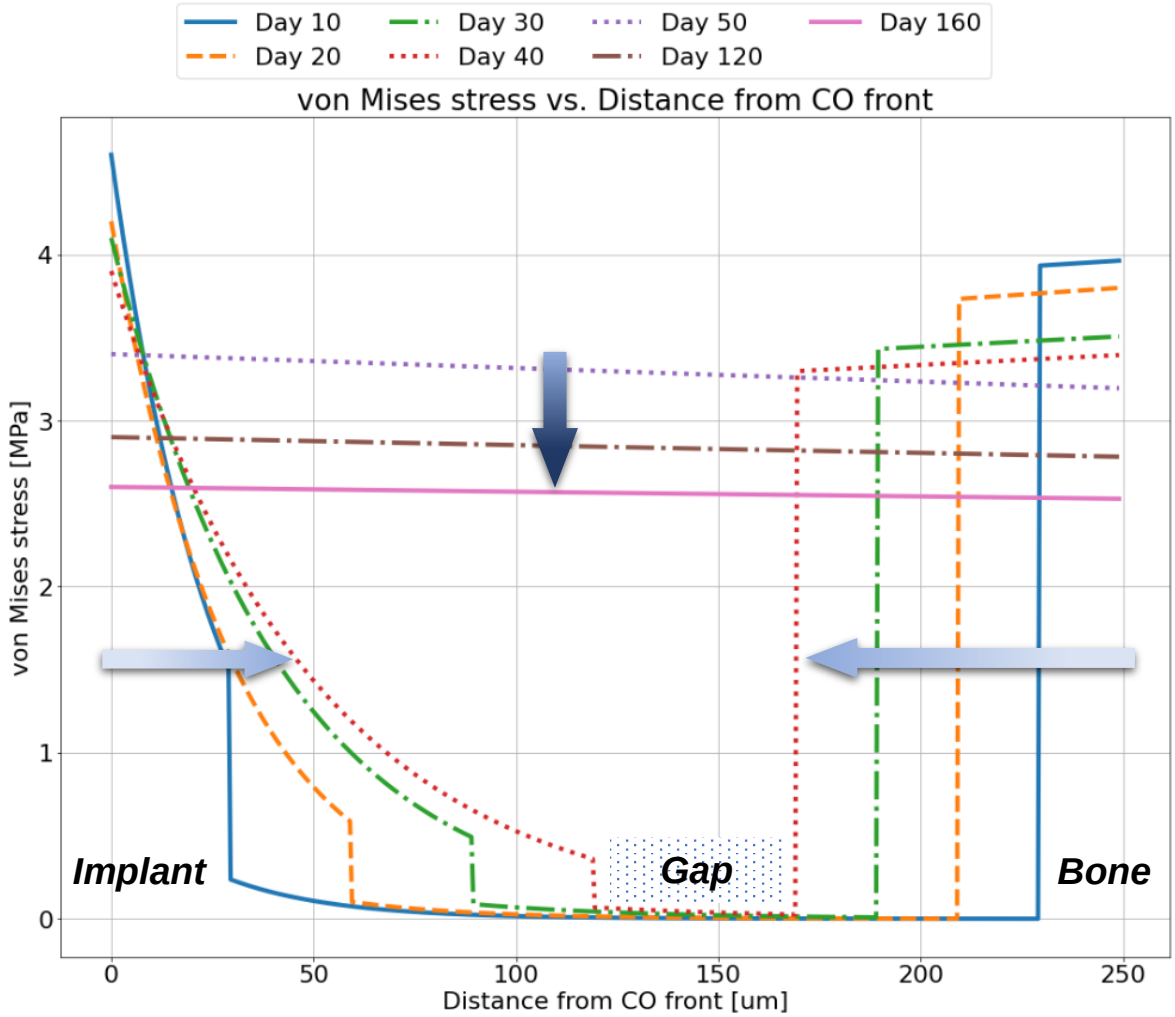

Figure 8: The calculated von Mises stress as a function of the BII evolution.

Figure 8 shows that as long as the gap is not closed, there is a significant stress gradient on both CO and DO sides, separated by a minimally stressed gap. Upon closure (day 50), the stress distribution changes significantly, becoming almost constant in the BII with a tendency to decrease when time elapses and the stiffness increases.

5.2 Resonance frequency analysis

The RFA results were calculated individually at every time step.

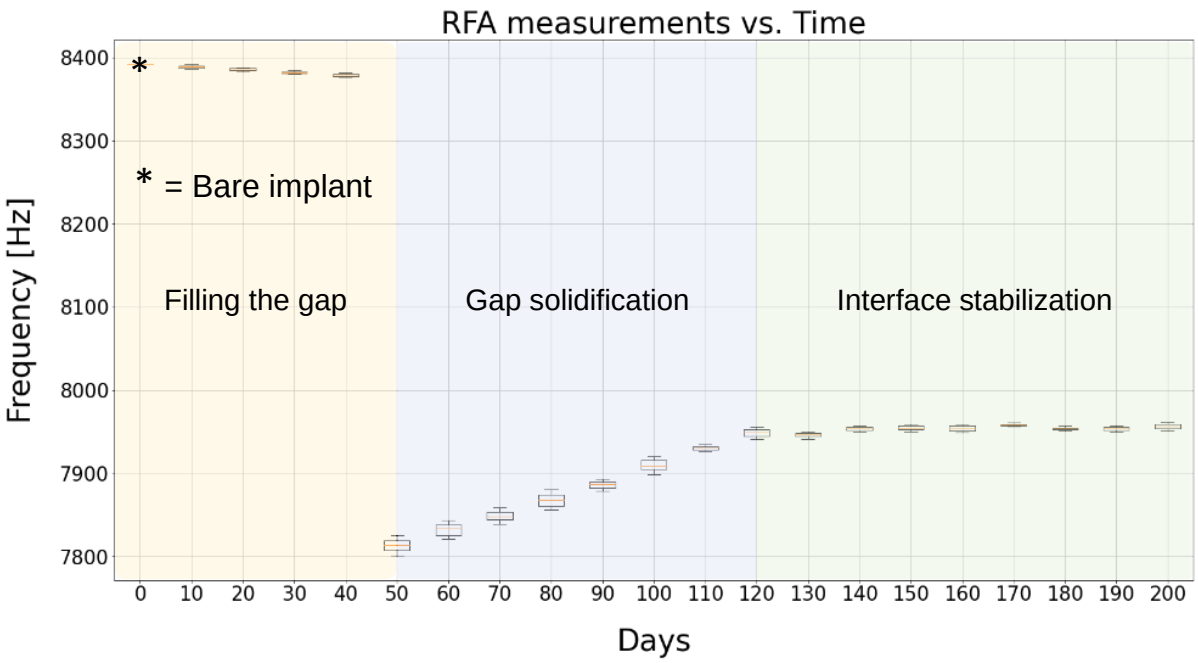

Figure 9: Boxplot of the resonance frequency (first mode) of the bone-implant ensemble as a function of time. At day 0, the reported frequency is that of the bare implant.

First, one can note that the range of resonant frequencies is quite narrow, not exceeding 600 Hz, with the highest frequency being characteristic of the bare implant. As long as the gap is not closed (day < 50), the change in resonant frequency is hardly detectable and remains close to that of the bare implant. Once it is closed, the resonant frequency drops dramatically to an average value of 7813 Hz. As the ensemble becomes stiffer due to gap "solidification", the resonance increases as expected, until it reaches a plateau around day 120. Note that by that time, there are no changes in BIC and the interfacial stiffness, as appears in Figure 3.

6. Discussion

In this paper, we developed a finite element model with explicit modelling of the BII spatial-temporal evolution based on CO/DO concepts. This model is a continuation of the basic interface modelling of Xie et al. [26], albeit applied now to a three-dimensional implant geometry. It can be argued that the physical (biological) reality of such an interface is much more complex, starting at the nanoscale. Likewise, different models of osseointegration can be found that provide detailed biological information on the nature of the bone-implant interface, such as soft tissue and bone debris, in

addition to new/old bone[53]. All in all, and despite the detailed information, such models can be simplified to the gap reduction until closure and tissue stiffening. With that, a model that encompasses all scales, from nano to macroscopic, is currently beyond reach, whereas a homogenized model of the kind developed here, in which the salient features of the osseointegration process (the kinematics and the statics), can provide useful and clinically relevant insights.

The first remark that can be made is that when one compares the rates of osseointegration expressed via the BIC percentage, alongside the CO/DO kinetics, it is evident that the BIC reaches its maximal value long before the interfacial gap closure is achieved. The BIC evolves on the CO (implant) side while it is constant ("perfect") on the DO (bone) side. Due to this difference in kinematics, one can decouple BIC and interfacial strength. Whereas the former reaches early completion, the latter starts manifesting itself only when the interfacial gap closure is achieved. As illustrated in Figure 8, the stress transmission across the interface is, to some extent, nonexistent as long as the gap remains open. Consequently, the sole characterization of the BIC is insufficient to determine the mechanical response of the BII. It is also interesting to note that once the gap is closed, the equivalent stress in the BII is almost constant, getting lower in time as the BII stiffness increases.

The next point worth being addressed is that of the resonant frequency. Figure 9 shows again a marked difference before and after gap closure. Before gap closure, the essential mechanical actor is the (bare) implant which is weakly connected to its surroundings. However, once the gap is closed, the resonant structure is composed of implant, BII and bone. This ensemble is of course less stiff (and heavier) than the sole implant, which explains the sudden drop in resonant frequency. But as the BII stiffens due to the increase in newly formed bone and decrease in soft tissue and bone debris[53], the resonant frequency increases mildly as expected. However, the calculated gap of frequency is some 150 Hz, which may be quite delicate to evaluate reliably with repeatability. Finally, past day 130, the RFA will not reveal any new evolution. This result is coherent with the BII unchanged stiffness during this time period.

In other words, as long as the gap exists and the BIC is still evolving, early RFA measurements are insensitive. The drop in Figure 9 may reveal complete gap closure which is of clinical importance. The maturation of the BII will be embodied in the frequency increase, irrespective of the BIC which is constant. Some validation of this result can be found in the many clinical measurements of RFA that report a similar behavior of the frequency evolution over time[19,54–58].

7. Conclusions

The results of this study point to two important and previously un-noticed points: While two characteristics can describe the bone-implant interface, namely the BIC on the implant side and the stiffness of the BIII, it appears that the BIC reaches completion long before the interfacial gap of the BII has closed.

Consequently, the discontinuity between the bone and the implant hampers load transmission until the gap is closed, thereby turning the BIC concept into secondary.

Once the gap is closed the interfacial stress becomes quite uniform, decreasing in time as the interface stiffens.

The outcome of those mechanical evolutions translates at the RFA level by an initially high frequency (akin ISQ) which characterizes the bare implant while the gap is open. As soon as the gap closes, the frequency drops down as a full solid unit is formed, rising slowly as the interfacial element stiffens.

The overall range of variation of the calculated frequencies reveals potential experimental difficulties in terms of resolution.

The comparison of the calculated resonant frequencies lines qualitatively with reported clinical RFA measurements, both in terms of frequency values (when reported) and their evolution with time, thereby validating the present model and the underlying assumptions.

Declaration of Competing Interest

The authors declare they have no conflict of interest whatsoever.

Bibliography

1. Steigenga JT, Al-Shammari KF, Nociti FH, Misch CE, Wang HL. Dental implant design and its relationship to long-term implant success. *Implant Dent*. 2003;12(4):306-317. doi:10.1097/01.ID.0000091140.76130.A1
2. Albrektsson T, Brånemark PI, Hansson HA, Lindström J. Osseointegrated titanium implants: Requirements for ensuring a long-lasting, direct bone-to-implant anchorage in man. *Acta Orthop*. 1981;52(2):155-170. doi:10.3109/17453678108991776
3. Swami V, Vijayaraghavan V, Swami V. Current trends to measure implant stability. *J Indian Prosthodont Soc*. 2016;16(2):124-130. doi:10.4103/0972-4052.176539
4. Soballe K, Hansen ES, Brockstedt-Rasmussen H, Bunger C. Hydroxyapatite coating converts fibrous tissue to bone around loaded implants. *J Bone Jt Surg - Ser B*. 1993;75(2):270-278. doi:10.1302/0301-620x.75b2.8444949
5. Burr DB, Allen MR. Basic and Applied Bone Biology. *Basic Appl Bone Biol*. Published online 2013:1-373. doi:10.1016/C2011-0-05817-9
6. Slyfield CR, Tkachenko E V., Wilson DL, Hernandez CJ. Three-dimensional dynamic bone histomorphometry. *J Bone Miner Res*. 2012;27(2):486-495. doi:10.1002/jbmr.553
7. Gao X, Fraulob M, Haïat G. Biomechanical behaviours of the bone-implant interface: A review. *J R Soc Interface*. 2019;16(156). doi:10.1098/rsif.2019.0259
8. Nkenke E, Hahn M, Weinzierl K, Radespiel-Tröger M, Neukam FW, Engelke K. Implant stability and histomorphometry: A correlation study in human cadavers using stepped cylinder implants. *Clin Oral Implants Res*. 2003;14(5):601-609. doi:10.1034/j.1600-0501.2003.00937.x
9. Mora-Macías J, Reina-Romo E, López-Pliego M, Giráldez-Sánchez MA, Domínguez J. In Vivo Mechanical Characterization of the Distraction Callus During Bone Consolidation. *Ann Biomed Eng*. 2015;43(11):2663-2674. doi:10.1007/s10439-015-1330-7
10. Mora-Macías J, Reina-Romo E, Domínguez J. Model of the distraction callus tissue behavior during bone transport based in experiments in vivo. *J Mech Behav Biomed Mater*. 2016;61:419-430. doi:10.1016/j.jmbbm.2016.04.016
11. Iezzi G, Degidi M, Piattelli A, Shibli JA, Perrotti V. A histological and histomorphometrical evaluation of retrieved human implants with a wettable, highly hydrophilic, hierarchically microstructured surface: A retrospective analysis of 14 implants. *Implant Dent*. 2013;22(2):138-142. doi:10.1097/ID.0b013e3182828114
12. Degidi M, Piattelli A, Shibli JA, Perrotti V, Iezzi G. Bone formation around immediately loaded and submerged dental implants with a modified sandblasted and acid-etched surface after 4 and 8 weeks: a human histologic and histomorphometric analysis. *Int J Oral Maxillofac*

Implants. 2009;24(5):896-901. http://www.ncbi.nlm.nih.gov/pubmed/19865630

13. Merdith, Neil;Book,K;Friberg,B;Jemt,T; Sennerby L. Resonance frequency measurements of implant stability in vivo. *Clin Oral Implants Res*. 1997;8:226-233.
14. Rittel D, Dorogoy A, Haïat G, Shemtov-Yona K. Resonant frequency analysis of dental implants. *Med Eng Phys*. 2019;66:65-74. doi:10.1016/j.medengphy.2019.02.008
15. Oh JS, Kim SG, Lim SC, Ong JL. A comparative study of two noninvasive techniques to evaluate implant stability: Periotest and Osstell Mentor. *Oral Surgery, Oral Med Oral Pathol Oral Radiol Endodontology*. 2009;107(4):513-518. doi:10.1016/j.tripleo.2008.08.026
16. Akkocaoglu M, Uysal S, Tekdemir I, Akca K, Cehreli MC. Implant design and intraosseous stability of immediately placed implants: A human cadaver study. *Clin Oral Implants Res*. 2005;16(2):202-209. doi:10.1111/j.1600-0501.2004.01099.x
17. Sennerby L, Meredith N. Implant stability measurements using resonance frequency analysis: Biological and biomechanical aspects and clinical implications. *Periodontol 2000*. 2008;47(1):51-66. doi:10.1111/j.1600-0757.2008.00267.x
18. H H, G W, E H. The clinical significance of implant stability quotient (ISQ) measurements: A literature review. *J Oral Biol Craniofacial Res*. 2020;10(4):629-638. doi:10.1016/j.jobcr.2020.07.004
19. Huwiler MA, Pjetursson BE, Bosshardt DD, Salvi GE, Lang NP. Resonance frequency analysis in relation to jawbone characteristics and during early healing of implant installation. *Clin Oral Implants Res*. 2007;18(3):275-280. doi:10.1111/j.1600-0501.2007.01336.x
20. Scarano A, Degidi M, Iezzi G, Petrone G, Piattelli A. Correlation between implant stability quotient and bone-implant contact: A retrospective histological and histomorphometrical study of seven titanium implants retrieved from humans. *Clin Implant Dent Relat Res*. 2006;8(4):218-222. doi:10.1111/j.1708-8208.2006.00022.x
21. Makary C, Rebaudi A, Sammartino G, Naaman N. Implant primary stability determined by resonance frequency analysis: Correlation with insertion torque, histologic bone volume, and torsional stability at 6 weeks. *Implant Dent*. 2012;21(6):474-480. doi:10.1097/ID.0b013e31826918f1
22. Rocci A, Martignoni M, Burgos PM, Gottlow J, Sennerby L. Histology of retrieved immediately and early loaded oxidized implants: Light microscopic observations after 5 to 9 months of loading in the posterior mandible. *Clin Implant Dent Relat Res*. 2003;5(SUPPL. 1):88-98. doi:10.1111/j.1708-8208.2003.tb00020.x
23. Zanetti EM, Ciaramella S, Calì M, et al. Modal analysis for implant stability assessment: Sensitivity of this methodology for different implant designs. *Dent Mater*. 2018;34(8):1235-

1245. doi:10.1016/j.dental.2018.05.016

24. Natali AN, Pavan PG, Ruggero AL. Analysis of bone-implant interaction phenomena by using a numerical approach. *Clin Oral Implants Res*. 2006;17(1):67-74. doi:10.1111/j.1600-0501.2005.01162.x

25. Puleo DA, Nanci A. Understanding and controlling the bone-implant interface. *Biomaterials*. 1999;20(23-24):2311-2321. doi:10.1016/S0142-9612(99)00160-X

26. Xie J, Rittel D, Shemtov-Yona K, Shah FA, Palmquist A. A stochastic micro to macro mechanical model for the evolution of bone-implant interface stiffness. *Acta Biomater*. 2021;131:415-423. doi:10.1016/j.actbio.2021.06.019

27. Davies JE. Bone bonding at natural and biomaterial surfaces. *Biomaterials*. 2007;28(34):5058-5067. doi:10.1016/j.biomaterials.2007.07.049

28. Trisi P, Lazzara R, Rao W, Rebaudi A. Bone-implant contact and bone quality: evaluation of expected and actual bone contact on machined and osseotite implant surfaces. *Int J Periodontics Restorative Dent*. 2002;22(6):535-545. doi:10.11607/prd.00.0501

29. Degidi M, Piattelli A, Shibli JA, Perrotti V, Iezzi G. Early bone formation around immediately restored implants with and without occlusal contact: A human histologic and histomorphometric evaluation. case report. *Int J Oral Maxillofac Implant*. 2009;24(4):734-739.

30. Iezzi G, Degidi M, Shibli J, Vantaggiato G, Piattelli A, Perrotti V. Bone Response to Dental Implants After a 3- to 10-Year Loading Period: A Histologic and Histomorphometric Report of Four Cases. *Int J Periodontics Restorative Dent*. 2013;33(6):755-761. doi:10.11607/prd.1257

31. Shibli JA, Mangano C, Mangano F, et al. Bone-to-Implant Contact Around Immediately Loaded Direct Laser Metal-Forming Transitional Implants in Human Posterior Maxilla. *J Periodontol*. 2013;84(6):732-737. doi:10.1902/jop.2012.120126

32. Bezerra Ferreira JD, Rodrigues JA, Piattelli A, Iezzi G, Gehrke SA, Shibli JA. The effect of cigarette smoking on early osseointegration of dental implants: a prospective controlled study. *Clin Oral Implants Res*. 2016;27(9):1123-1128. doi:10.1111/clr.12705

33. Mangano FG, Iezzi G, Shibli JA, et al. Early bone formation around immediately loaded implants with nanostructured calcium-incorporated and machined surface: a randomized, controlled histologic and histomorphometric study in the human posterior maxilla. *Clin Oral Investig*. 2017;21(8):2603-2611. doi:10.1007/s00784-017-2061-y

34. Shibli JA, Grassi S, De Figueiredo LC, Feres M, Iezzi G, Piattelli A. Human peri-implant bone response to turned and oxidized titanium implants inserted and retrieved after 2 months. *Implant Dent*. 2007;16(3):252-259. doi:10.1097/ID.0b013e3180de4d64

35. Mangano FG, Pires JT, Shibli JA, et al. Early Bone Response to Dual Acid-Etched and Machined Dental Implants Placed in the Posterior Maxilla: A Histologic and Histomorphometric Human Study. *Implant Dent*. 2017;26(1):24-29. doi:10.1097/ID.0000000000000511
36. Orsini G, Piattelli M, Scarano A, et al. Randomized, Controlled Histologic and Histomorphometric Evaluation of Implants With Nanometer-Scale Calcium Phosphate Added to the Dual Acid-Etched Surface in the Human Posterior Maxilla. *J Periodontol*. 2007;78(2):209-218. doi:10.1902/jop.2007.060297
37. Shibli JA, Grassi S, De Figueiredo LC, et al. Influence of implant surface topography on early osseointegration: A histological study in human jaws. *J Biomed Mater Res - Part B Appl Biomater*. 2007;80(2):377-385. doi:10.1002/jbm.b.30608
38. Shibli JA, Piattelli A, Iezzi G, et al. Effect of Smoking on Early Bone Healing Around Oxidized Surfaces: A Prospective, Controlled Study in Human Jaws. *J Periodontol*. 2010;81(4):575-583. doi:10.1902/jop.2010.090493
39. d'Avila S, dos Reis LD, Piattelli A, et al. Impact of smoking on human bone apposition at different dental implant surfaces: a histologic study in type IV bone. *J Oral Implantol*. 2010;36(2):85-90. doi:10.1563/AAID-JOI-D-09-00018
40. Mangano C, Piattelli A, d'Avila S, et al. Early human bone response to laser metal sintering surface topography: a histologic report. *J Oral Implantol*. 2010;36(2):91-96. doi:10.1563/AAID-JOI-D-09-00003
41. Yonezawa D, Piattelli A, Favero R, Ferri M, Iezzi G, Botticelli D. Bone Healing at Functionally Loaded and Unloaded Screw-Shaped Implants Supporting Single Crowns: A Histomorphometric Study in Humans. *Int J Oral Maxillofac Implants*. 2018;33(1):181-187. doi:10.11607/jomi.5928
42. Traini T, Pecora G, Iezzi G, Piattelli A. Preferred collagen fiber orientation human peri-implant bone after a short- and long-term loading period: a case report. *J Oral Implantol*. 2006;32(4):177-181. doi:10.1563/285.1
43. Iezzi G, Degidi M, Scarano A, Perrotti V, Piattelli A. Bone response to submerged, unloaded implants inserted in poor bone sites: a histological and histomorphometrical study of 8 titanium implants retrieved from man. *J Oral Implantol*. 2005;31(5):225-233. doi:10.1563/1548-1336(2005)31[225:BRTSUI]2.0.CO;2
44. Testori T, Szmukler-Monder S, Francetti L, et al. Immediate Loading of Osseotite Implants: A Case Report and Histologic Analysis after 4 Months of Occlusal Loading. *Int J Periodontics Restor Dent*. 2001;21(5):451-459. doi:10.11607/prd.00.0437
45. Degidi M, Petrone G, Iezzi G, Piattelli A. Bone contact around acid-etched implants: a

histological and histomorphometrical evaluation of two human-retrieved implants. *J Oral Implantol*. 2003;29(1):13-18. doi:10.1563/1548-1336(2003)029<0013:BCAAIA>2.3.CO;2

46. Degidi M, Petrone G, Iezzi G, Piattelli A. Histologic evaluation of a human immediately loaded titanium implant with a porous anodized surface. *Clin Implant Dent Relat Res*. 2002;4(2):110-114. doi:10.1111/j.1708-8208.2002.tb00160.x
47. Degidi M, Scarano A, Iezzi G, Piattelli A. Periimplant Bone in Immediately Loaded Titanium Implants: Histologic and Histomorphometric Evaluation in Human. A Report of Two Cases. *Clin Implant Dent Relat Res*. 2003;5(3):170-175. doi:10.1111/j.1708-8208.2003.tb00199.x
48. Mangano C, Shibli JA, Pires JT, Luongo G, Piattelli A, Iezzi G. Early Bone Formation around Immediately Loaded Transitional Implants Inserted in the Human Posterior Maxilla: The Effects of Fixture Design and Surface. *Biomed Res Int*. 2017;2017:4-6. doi:10.1155/2017/4152506
49. Iezzi G, Fiera E, Scarano A, Pecora G, Piattelli A. Histologic evaluation of a provisional implant retrieved from man 7 months after placement in a sinus augmented with calcium sulphate: a case report. *J Oral Implantol*. 2007;33(2):89-95. doi:10.1563/0.808.1
50. MIS SEVEN - Internal Hexagon Implant System | MIS Dental Implants. Accessed June 22, 2022. https://www.mis-implants.com/products/implant-systems/seven
51. Guan H, Van Staden RC, Johnson NW, Loo YC. Dynamic modelling and simulation of dental implant insertion process-A finite element study. *Finite Elem Anal Des*. 2011;47(8):886-897. doi:10.1016/j.finel.2011.03.005
52. ABAQUS. Abaqus 6.14 Documentation. *Abaqus 614 Anal User's Guid*. Published online 2014:14. Accessed July 17, 2022. http://130.149.89.49:2080/v6.14/
53. Lang NP, Berglundh T, Giannobile W V, Sanz M. *Lindhe's Clinical Periodontology and Implant Dentistry, 2 Volume Set*. (Niklaus P. Lang, Tord Berglundh, William V. Giannobile MS, ed.). John Wiley & Sons; 2021.
54. Friberg B, Sennerby L, Linden B, Gröndahl K, Lekholm U. Stability measurements of one-stage Brånemark implants during healing in mandibles. *Int J Oral Maxillofac Surg*. 1999;28(4):266-272. doi:10.1016/s0901-5027(99)80156-8
55. Ersanli S, Karabuda C, Beck F, Leblebicioglu B. Resonance Frequency Analysis of One- Stage Dental Implant Stability During the Osseointegration Period. *J Periodontol*. 2005;76(7):1066-1071. doi:10.1902/jop.2005.76.7.1066
56. Glauser R, Sennerby L, Meredith N, et al. Resonance frequency analysis of implants subjected to immediate or early functional occlusal loading. Successful vs. failing implants. *Clin Oral Implants Res*. 2004;15(4):428-434. doi:10.1111/j.1600-0501.2004.01036.x

57. Crismani AG, Bernhart T, Schwarz K, Čelar AG, Bantleon HP, Watzek G. Ninety percent success in palatal implants loaded 1 week after placement: A clinical evaluation by resonance frequency analysis. *Clin Oral Implants Res*. 2006;17(4):445-450. doi:10.1111/j.1600-0501.2005.01223.x

58. Kittur N, Oak R, Dekate D, Jadhav S, Dhatrak P. Dental implant stability and its measurements to improve osseointegration at the bone-implant interface: A review. *Mater Today Proc*. 2020;43:1064-1070. doi:10.1016/j.matpr.2020.08.243

Appendix

1. von Mises stresses as a function of time and distance

Figure 8 shows lack of symmetry of the calculated von Mises stress on the implant and the bone sides. We assume this phenomenon is caused by the stiffness difference between the implant and the bone, resulting in a different kind of constraint. To properly validate this assumption, an additional set of calculations is run with identical mechanical properties assigned to the bone and the implant (both titanium). As shown in Figure A1, the calculated von Mises stress for three different time steps, indicate a highly symmetrical state of stress on both sides, thereby validating the above assumption.

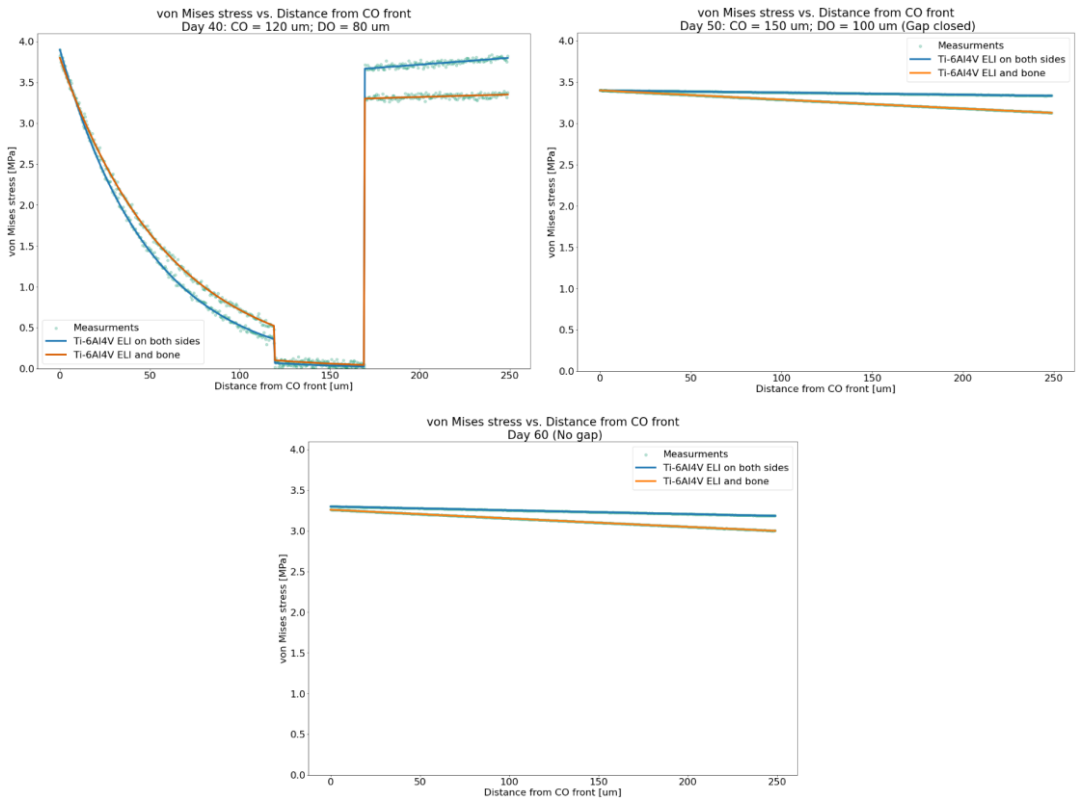

Figure A.1: The calculated von Mises stress for identical mechanical properties of the bone and the implant.